1. ODE MODEL PARAMETERIZATION

Table S1: Sources of default parameter values used in the ODE model simulations. Parameters whose values were varied (u, ε_s, ε_d, c_s, and c_d) are not shown. Code for all calculations is available at https://doi.org/10.5281/zenodo.8317545.

Parameter	Description	Units	Default Value	Source
r_G	Gametophyte maturation rate	d^{-1}	0.05	Deysher & Dean 1984, Reed et al. 1994
μ_G	Gametophyte mortality rate	G^{-1} d^{-1}	0.6	Reed 1990
r_J	Juvenile sporophyte maturation rate	d^{-1}	0.004	Dayton et al. 1984
μ_J	Juvenile sporophyte mortality rate	J^{-1} d^{-1}	0.01	Dayton et al. 1984
K	Adult sporophyte carrying capacity	ind m^{-2}	1	Reed et al. 1988
μ_A	Adult sporophyte mortality rate	d^{-1}	0.002	SBC LTER et al. 2023a[a]
b	Biomass per adult sporophyte	kg ind^{-1}	7	SBC LTER 2022a[b], Kushner et al. 2013[c], SBC LTER et al. 2023a[a]
ρ	Adult sporophyte spore production rate	spores kg^{-1} d^{-1}	10	Estimated within model[e]
d	Adult sporophyte drift production rate	kg drift kg^{-1} d^{-1}	0.024	SBC LTER et al. 2023a[a]
g_d	Rate of drift consumption by urchins	kg drift u^{-1} d^{-1}	0.0011	DiFiore et al. 2021[d]
g	Max. grazing rate on adult sporophytes	ind u^{-1} d^{-1}	0.025	Karatayev et al. 2021
q_G	Grazing vulnerability of gametophytes relative to adults (max. grazing rate = $q_G g$)	–	1.2	Karatayev et al. 2021
q_J	Grazing vulnerability of juvenile sporophytes relative to adults (max.grazing rate = $q_J g$)	–	1.2	Karatayev et al. 2021
p	Reduction in grazing (relative to max.) if rates of drift production and consumption are equal	–	0.1	Karatayev et al. 2021
l_s	Fraction locally produced spores that leave patch	–	0.5	[f]
l_d	Fraction locally produced drift that leaves patch	–	0.5	[f]

[a]Dataset includes monthly plant loss rates (used to estimate μ_A) as well as blade and frond loss rates (used to estimate d) and regression parameters for relating frond counts to plant biomass (used to convert observations of number of fronds per plant to plant biomass b)
[b]Dataset includes observations of giant kelp density and size (number of fronds per plant)
[c]Data paper with "Giant kelp size frequency" dataset from the CINP KFMP (size is recorded as number of fronds per individual; I used regression parameters from [a] to convert this to biomass)
[d]Data on urchin drift consumption from mesocosm experiments performed by Rennick et al. 2022
[e]Values were chosen such that the model produced biologically reasonable dynamics
[f]Could take any value between 0 and 1; in the absence of data I chose 0.5 as a default

2. THEORETICAL ODE MODEL ANALYSES

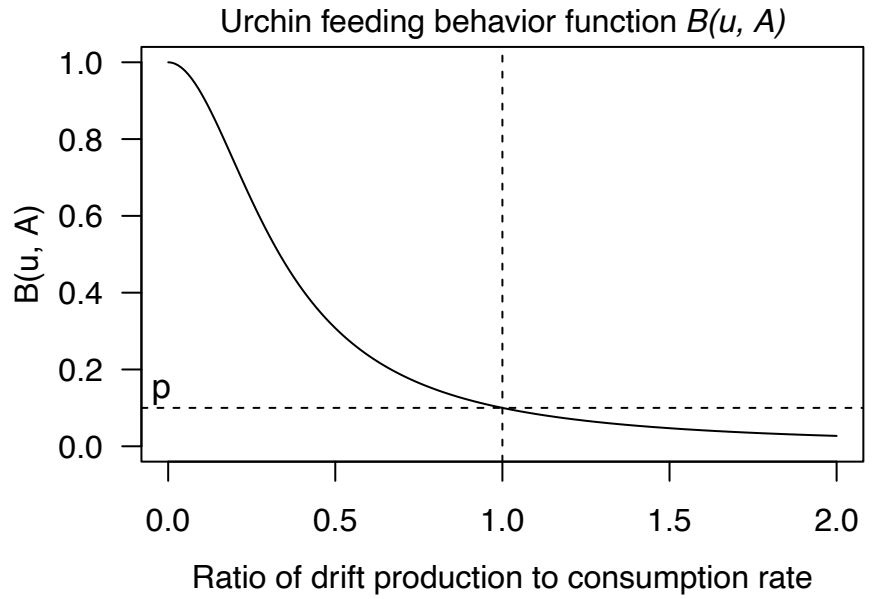

Figure S1: Urchin feeding behavior as a function of the ratio of drift production to consumption rates (where drift is produced by adult kelp sporophytes A and consumed by urchins u). The parameter p is the proportional reduction in maximum urchin grazing rate (herbivory) when rates of drift production and consumption are equal (e.g., a value of $p = 0.1$ means grazing is reduced to 10% of its maximum value when rates of drift production and consumption are equal).

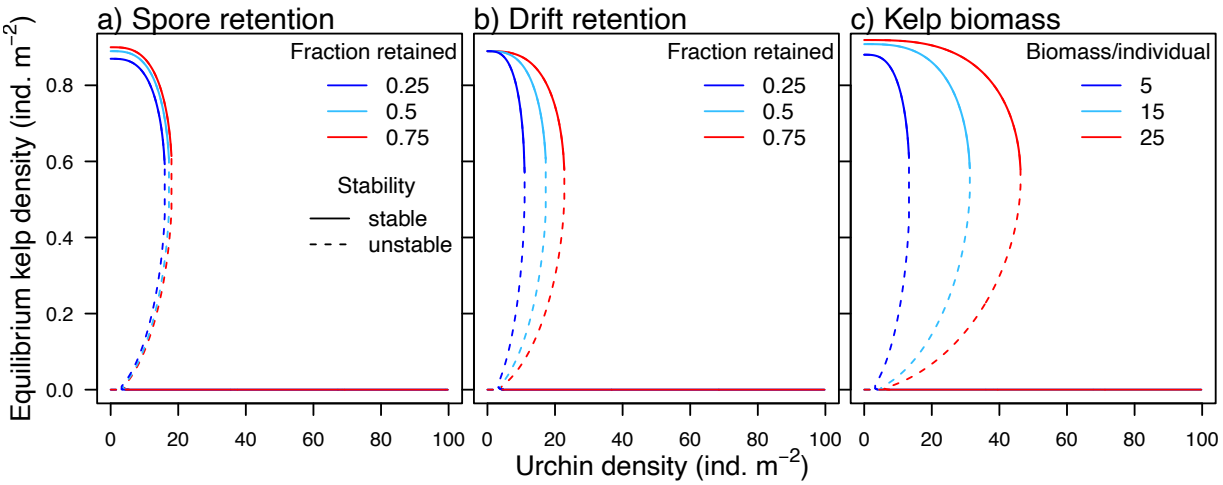

Figure S2: Effect of urchins, local retention rates, and kelp biomass on equilibrium kelp density. The x-axis is the density of urchins (u) and the y-axis is the equilibrium density of adult kelp sporophytes (A^*). Solid and dashed lines indicate stable and unstable equilibria, respectively. Line color represents a) fraction of spores retained in the patch ($1\text{-}l_s$), b) fraction of drift retained in the patch ($1\text{-}l_d$), or c) biomass per kelp plant (b; kg per individual). Higher values of plant biomass correspond to greater per-capita spore and drift production. There is no external input of spores or drift ($\varepsilon_s = \varepsilon_d = 0$).

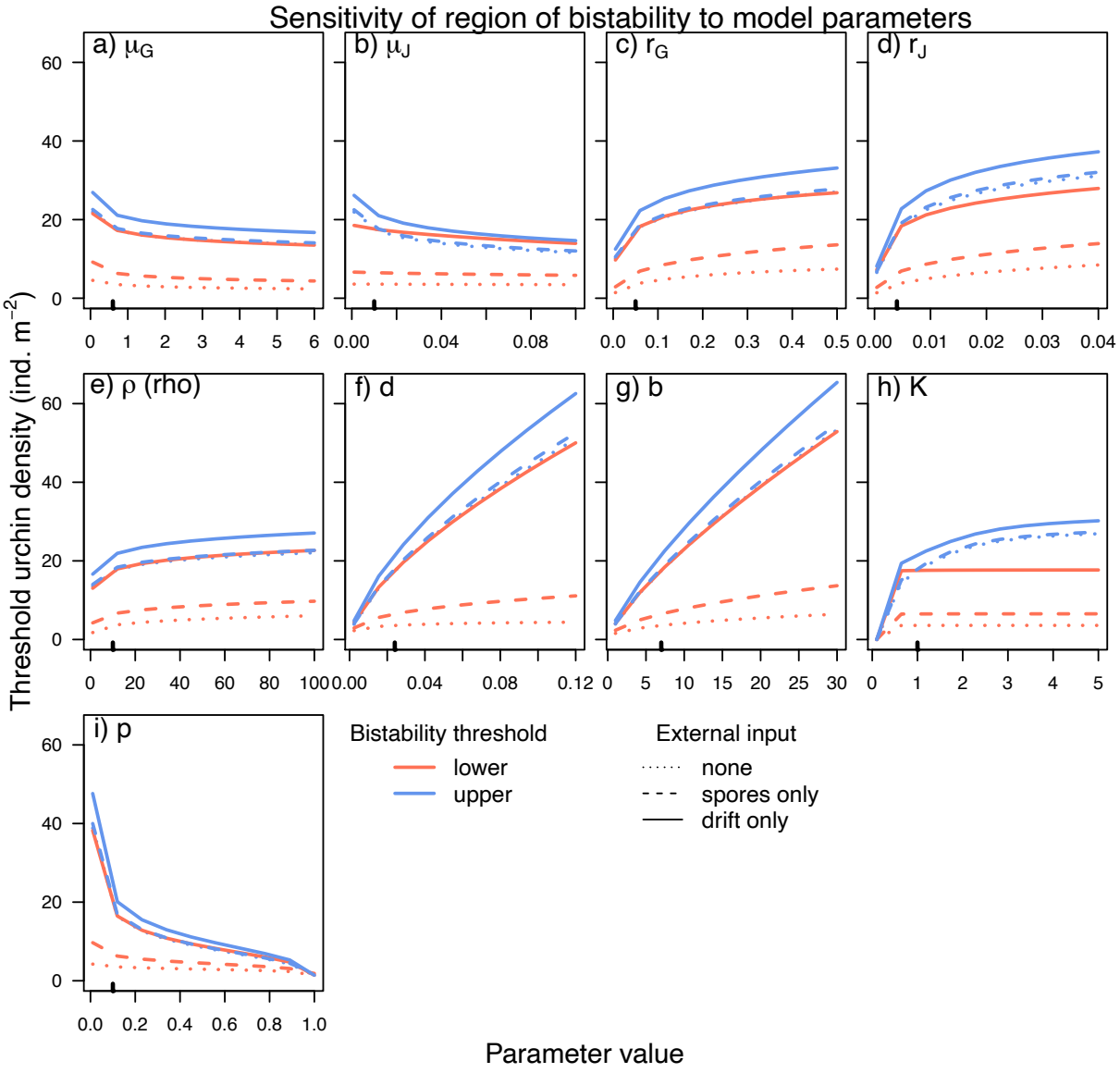

Figure S3: Effect of external spore or drift input and local model parameters on the region of bistability predicted by the ODE model. Dotted, dashed, and solid lines correspond to no external inputs ($\varepsilon_s = \varepsilon_d = 0$), input of spores only (ε_s = 0.2 x spore export rate of an urchin-free patch at equilibrium; $\varepsilon_d = 0$), and input of drift only ($\varepsilon_s = 0$; ε_d = 0.2 x drift export rate of an urchin-free patch at equilibrium), respectively. For each connectivity scenario, the red line is the lower bistability threshold (below this line, only the high kelp state is stable) and the blue line is the upper threshold (only the low kelp state is stable above this line). The system is bistable between the red and blue lines. Bold tick marks on the x-axes indicate the default value of each parameter.

Table S2: Sets of initial conditions used in the model simulations shown in Figure 3. The highest set corresponds to equilibrium densities (individuals m^{-2}) of each kelp life stage in an undisturbed, fully connected patch with no urchins (i.e., the highest possible densities for the default values of local parameters). For each intermediate value of A_0 (representing varying levels of disturbance), the corresponding values of J_0 and G_0 were calculated as functions of the proportional reduction in adult kelp density relative to its highest equilibrium value. If A_0 was at least 50% of its highest possible value, J_0 and G_0 were set to their highest values, otherwise, the fraction of these early life stages remaining after a disturbance was assumed to be 2x as high as that of adult kelp (as adult kelp's long fronds make it disproportionately susceptible to wave disturbance; Reed et al. 2011).

Initial Condition Set	A_0	J_0	G_0
lowest	0	0	10^{-4}
intermediate	variable	$\max(1, 2A_0/0.9)*4.9$	$\max(1, 2A_0/0.9)*10.2$
highest	0.9	4.9	10.2

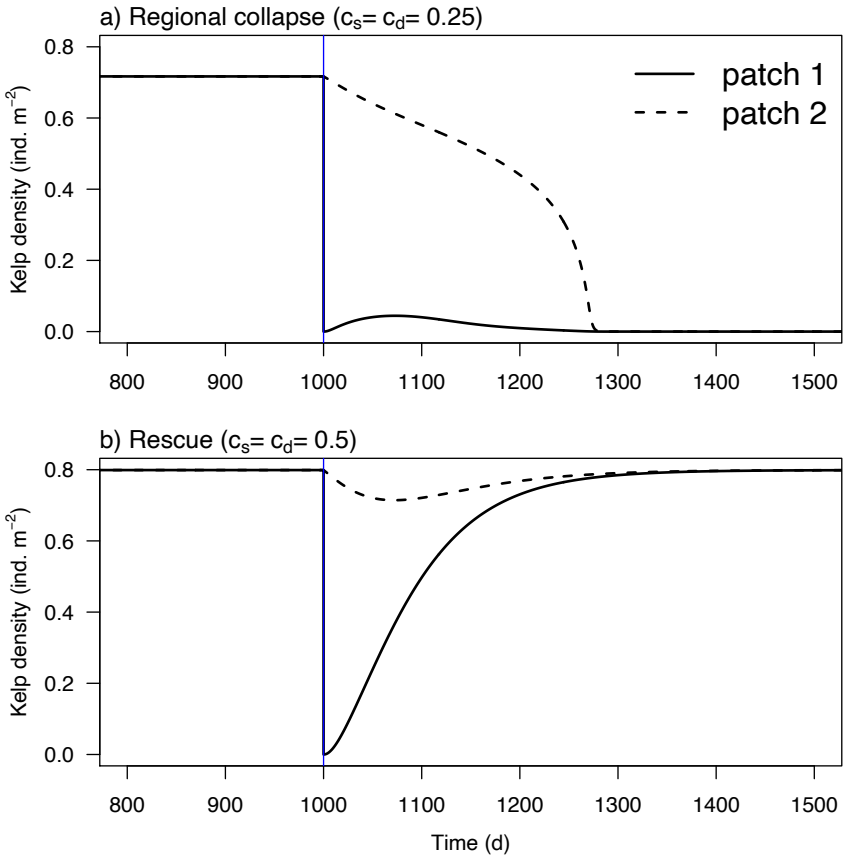

Figure S4: Time series illustrating two scenarios from Fig. 3c (spore and drift connectivity with local disturbance). In both a) and b), patch 1 experiences a major disturbance (blue vertical lines) while patch 2 is unaffected. Urchin density in both patches was set to 19 individuals m^{-2}. a) The

disturbance causes patch 1 to go to the low kelp state, and the loss of spore and drift input to patch 2 causes it to also collapse. b) At higher values of spore and drift connectivity, patch 1 receives sufficient levels of spore and drift input from patch 2 to enable it to quickly recover, and both patches end up in the high kelp state.

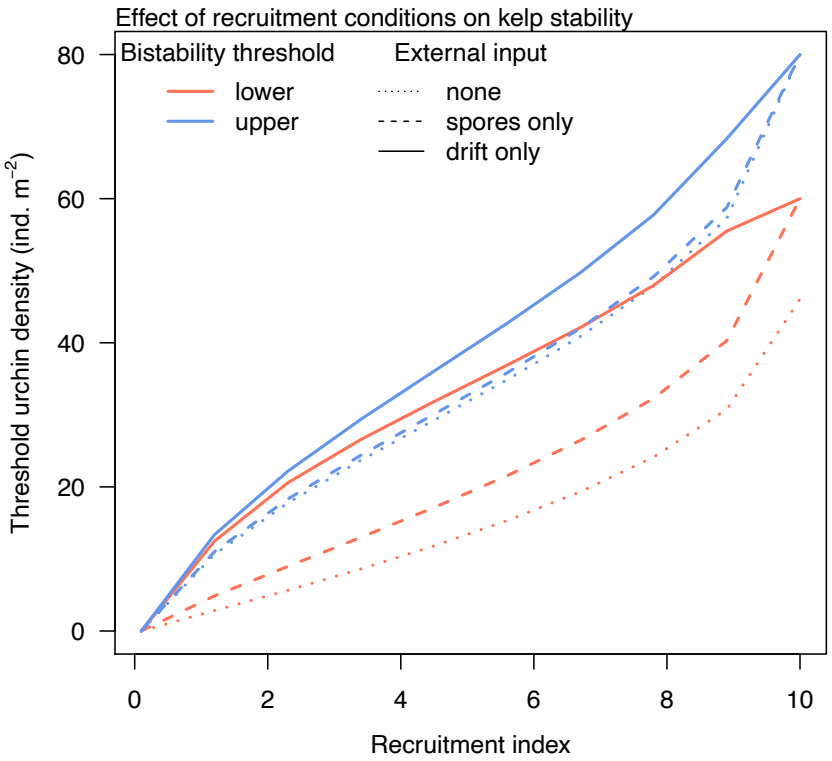

Figure S5: Effect of simultaneous variation in multiple recruitment parameters (spore production rate ρ, maturation rates r_G and r_J, and mortality rates μ_G and μ_J) on the region of bistability for different types of connectivity. Parameters were varied by multiplying their default values by a "recruitment index", ranging from 0.1 to 10. The mortality rates μ_G and μ_J were multiplied by the inverse of this index (as decreasing mortality rates indicate more favorable recruitment). Thus, an index of 10 means ρ, r_G and r_J are equal 10x their default values and μ_G and μ_J are equal 0.1x their default values. External input and the bistability thresholds are as defined in Fig. S3. All other parameters are at their default values (Table 1). Under the most favorable conditions (recruitment index = 10), external input of spores has approximately the same effect on kelp stability as external input of drift (dashed and solid lines meet); however, this set of parameter values produces unrealistically fast kelp dynamics if assumed constant (Fig. S6).

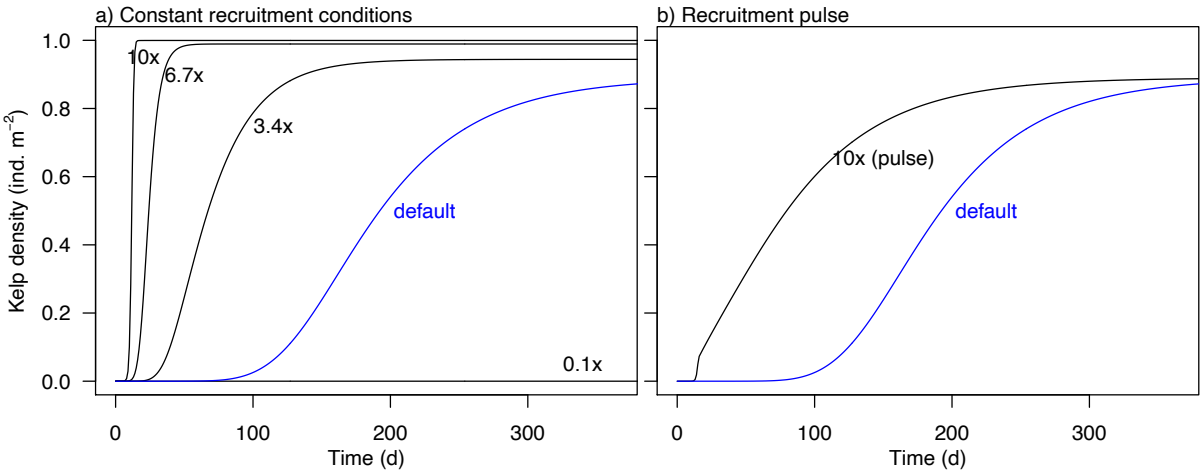

Figure S6: Effect of simultaneous variation in recruitment parameters (spore production rate ρ, maturation rates r_G and r_J, and mortality rates μ_G and μ_J) on giant kelp dynamics in the absence of connectivity. The default parameter set is shown in blue. The remaining simulations are labeled by the value of the "recruitment index" that multiplied the default recruitment parameters (e.g., 10x means ρ, r_G and r_J equal 10x their default values and μ_G and μ_J equal 0.1x their default values). a) All parameters were kept constant for each simulation. b) Increase in recruitment index from 1x to 10x occurred during only a brief window (days 5–12) before the recruitment parameters returned to their default values. In both a) and b), all other parameters are at their default values (Table 1). In favorable conditions, giant kelp is thought to take 6-9 months to develop from a spore to a mature, canopy-forming adult (Dayton et al. 1984); thus, the higher recruitment scenarios (10x, 6.7x) produce unrealistically fast dynamics in a) but could be reasonable if restricted to brief pulses as in b).

3. EMPIRICAL DATA

3.1 Transect-level data

The Santa Barbara Coastal Long Term Ecological Research site (SBC LTER) and Channel Islands National Park Kelp Forest Monitoring Program (CINP KFMP) conduct annual surveys of kelp forest communities at a total of 44 sites in and around the Santa Barbara Channel (Fig. S7). At each of these locations, divers record abundances of kelp forest species in quadrats and/or swaths positioned along one to several permanent transects. Surveys are performed in summer or early fall and, depending on the site, have been ongoing for 2–4 decades. From these data, I calculated annual transect-level urchin density as the sum of the densities of purple (*Strongylocentrotus purpuratus*) and red (*Mesocentrotus franciscanus*) urchins (the two dominant barren-forming species in this region; Harrold & Pearse 1987) within quadrats, averaged across all quadrats within a transect. For giant kelp, I used the density of kelp plants in contiguous swaths along the same transects. If kelp density in the transect was greater than 0.05 individuals m^{-2} (the 15th density quantile of all non-zero kelp densities), I classified the transect

as being in a "high kelp" state, otherwise I considered it to be in a "low kelp" state. Fig. 5b in the main text shows the resulting distributions of urchin densities and kelp states. I note there are instances where kelp was in the low state and there were no urchins; in these cases, the transect was not an urchin barren and kelp density was low for some other reason (e.g., high sand cover, lack of external spores for recolonization, etc.).

Full descriptions of these data and sampling methods are given by Kushner et al. 2013 (CINP KFMP data; see "Benthic density data" and "Giant kelp supplementary density data" sections) and SBC LTER et al. 2022a (SBC LTER giant kelp density data), SBC LTER et al. 2022c (SBC LTER benthic community survey data, including urchin densities), and SBC LTER et al. 2023b (LTER transect locations). In this study, I used the Southern California Bight Marine Biodiversity Observation Network's "Integrated Kelp forest/reef: Quad and Swath Survey" dataset, which includes all data from both the SBC LTER and CINP KFMP programs in a single dataset (SBC MBON et al. 2021).

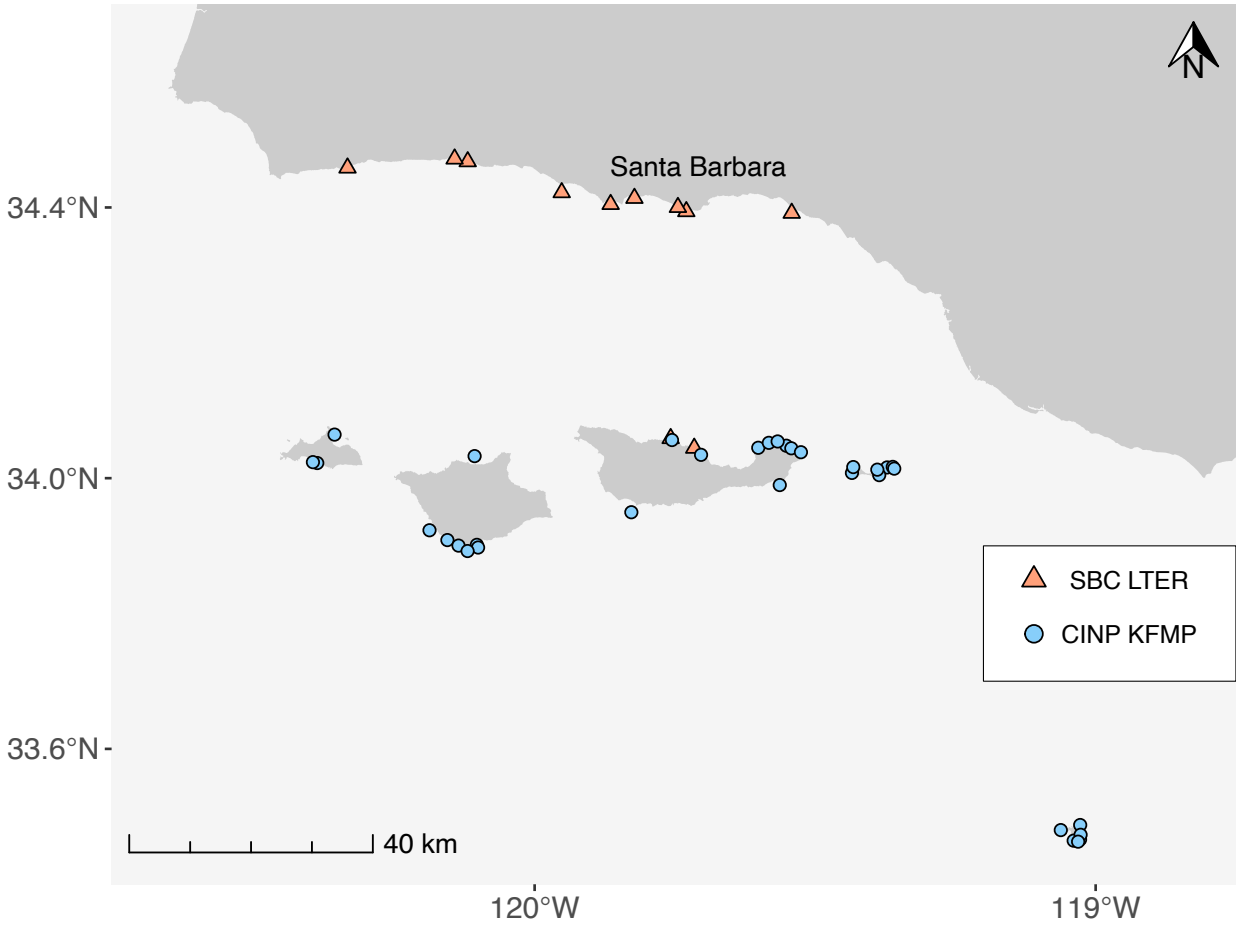

Figure S7: Map of the benthic monitoring sites. SBC LTER = Santa Barbara Coastal Long Term Ecological Research, CNIP KFMP = Channel Islands National Park Kelp Forest Monitoring Program.

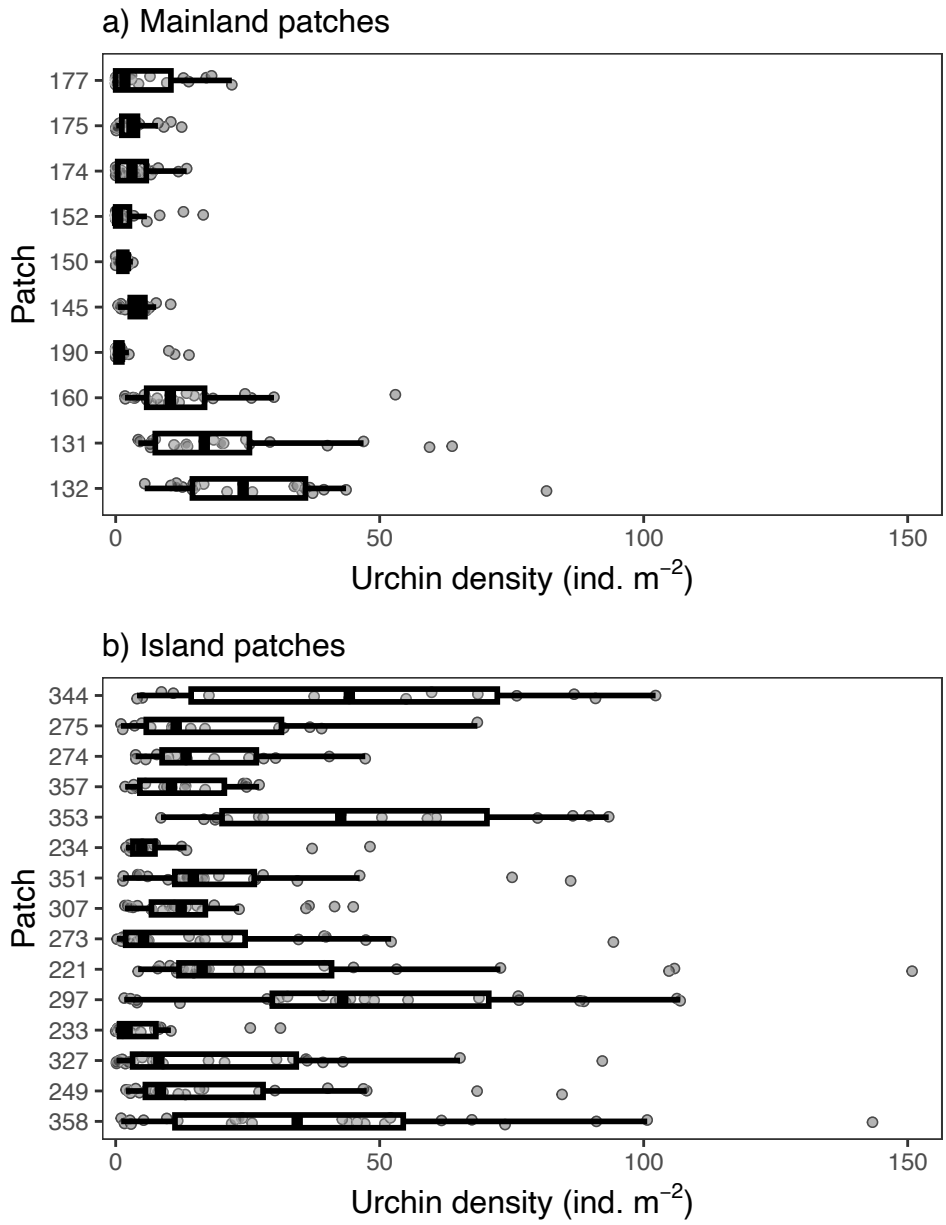

Figure S8: Distribution of urchin densities across the giant kelp metapopulation patches (arbitrarily numbered) containing benthic transects monitored by the SBC LTER and CINP KFMP. Each data point corresponds to observations in a single year. For patches containing more than one transect, the average urchin density across all transects in that year is shown. a) Patches along the mainland (Santa Barbara coastline). b) Patches along the four northern Channel Islands (San Miguel, Santa Rosa, Santa Cruz, and Anacapa) and Santa Barbara Island.

3.2 Patch-level data

To calculate metapopulation-scale characteristics of southern California kelp forests, I required data on kelp abundance at larger spatial scales than given by the benthic surveys described above. One well-developed approach for collecting this type of data is to estimate the biomass of a kelp forest's canopy (which, due to the buoyancy of giant kelp fronds, can be seen from the surface) from Landsat satellite images (see Cavanaugh et al. 2011 for a description of these methods). Landsat pixels cover the Southern California Bight with a spatial resolution of 30 m, and this method therefore provides estimates of kelp abundance throughout this entire region. By applying spatial autocorrelation and graph theory-based patch delineation algorithms to multi decadal Landsat data, Cavanaugh et al. (2014) were able to characterize the metapopulation structure of southern California kelp forests. The dynamics of this metapopulation are described in Castorani et al. (2015, 2017), and I used their published data in this study (Cavanaugh et al. 2019, Castorani et al. 2022b, 2022c).

The datasets referenced above include the location and area of every identified kelp patch in the southern California metapopulation (Fig. 5a), as well as the average canopy biomass and dispersal times among these patches in each semester between 1996-2006. The authors calculated a patch's biomass by summing the canopy biomass in all Landsat pixels within that patch and taking the average of this total over each semester. For dispersal time, the monthly minimum mean dispersal times between each pair of patches were estimated using Regional Oceanic Modeling System (ROMS) solutions for the Southern California Bight (Dong et al. 2009). Briefly, the authors released Lagrangian particles across a range of depths (5-30m) at 12 hour intervals in ROMS connectivity cells and used the particles' trajectories to calculate the minimum mean transit time of water parcels moving from one cell to another. The resulting transit times were assumed to be proportional to dispersal times between patches within these cells. For cases in which the distance between patches was smaller than the resolution of ROMS cells, linear interpolation was used to approximate dispersal times (see Castorani et al. 2022c for more details). As with biomass, dispersal times were averaged across each semester. I used these patch biomasses and dispersal times to calculate the semesterly connectivity of each metapopulation patch from 1996-2006 (eqn.s 13-14 in main text).

4. GLMM RESULTS AND ASSUMPTIONS

GLMM assumptions

The best-fitting GLMM included independent fixed effects of urchin density, patch connectivity, and patch area (Table S3). This model generally conformed well to model assumptions. Multicollinearity was low (variance inflation factors all <1.5; Zuur et al. 2009), the random effects were approximately normally distributed (Fig. S9), and there was no significant temporal or spatial autocorrelation in the residuals (Fig. S10). However, plotting the residuals against predicted values and against each fixed effect revealed several large outliers (Fig. S11). All were cases in which kelp was in the low state despite the transects having low urchin densities and being in relatively large, well-connected patches. I investigated the possibility that these low kelp densities could be due to unsuitable habitat (i.e., lack of hard substrate in the transects) using available SBC LTER data on benthic substrate composition (SBC LTER et al. 2022b). I found that high sand cover may explain two of the outliers (Fig. S13-14), but the others appear to be due to larger-scale processes affecting kelp populations at the patch level (e.g., oceanographic conditions or intra-annual cohort dynamics; Castorani et al. 2022, Nisbet & Bence 1989; Fig. S14). Removing the four outliers improved model residuals (Fig. S12) and had minimal effects on model fitting and predictions (Table S3, Fig. S15-17).

Table S3: Results of model selection for GLMMs fitted to the full dataset (left) and to the data set with outliers removed (right). Letters indicate fixed effects included in the model. U = urchin density, C = patch connectivity, A = patch area, and 0 = no fixed effects. UxC indicates an explicit interaction term between urchin density and patch connectivity.

	Full Data					No outliers			
	df	**AIC**	**delta**	**weights**		**df**	**AIC**	**delta**	**weights**
UCA	6	274.7	0	0.6	*UCA*	6	225.8	0	0.5
UxCA	7	276.7	2	0.2	*UxCA*	7	226.2	0.5	0.4
UC	5	278.9	4.2	0.1	*UC*	5	229.7	4	0.1
UxC	6	280.9	6.2	0	*UxC*	6	230	4.3	0.1
UA	5	284.3	9.6	0	*UA*	5	235.8	10	0
U	4	284.6	9.9	0	*U*	4	235.9	10.1	0
CA	5	313.1	38.4	0	*CA*	5	273.1	47.3	0
C	4	324.9	50.2	0	*C*	4	284	58.2	0
A	4	332.8	58.2	0	*A*	4	291.4	65.7	0
0	3	337.4	62.7	0	*0*	3	295.9	70.1	0

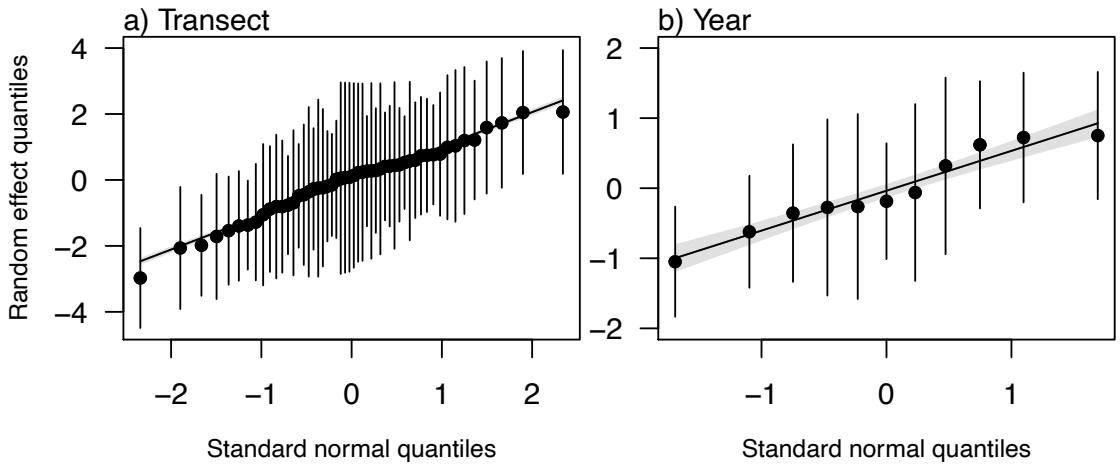

Figure S9: Quantile-quantile plots of the random effects in the GLMM model (transect and year). The solid line and gray shaded region are the predictions and 95% confidence intervals of a linear regression model fit through the points.

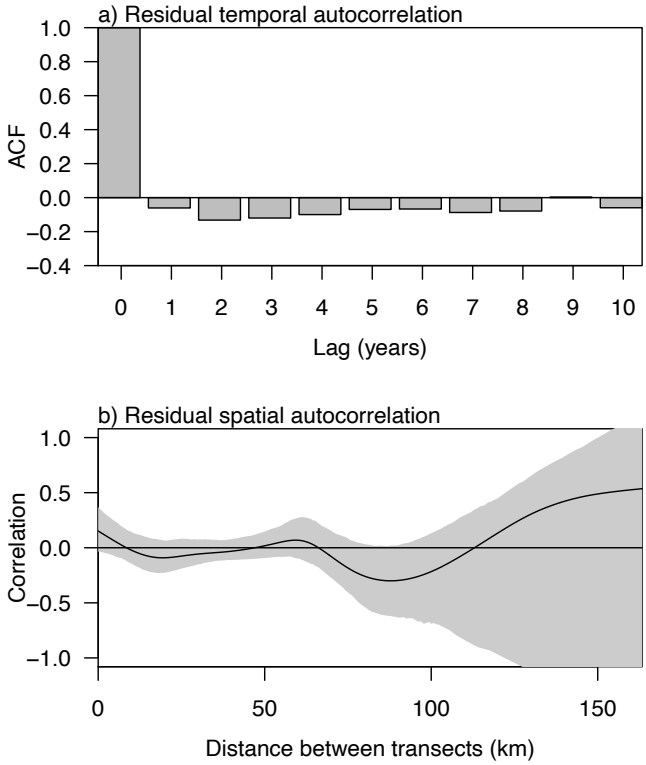

Figure S10: a) ACF plot of residuals (averaged across all transects) demonstrating no significant temporal autocorrelation among residuals. b) Spline correlogram demonstrating no significant spatial autocorrelation among residuals.

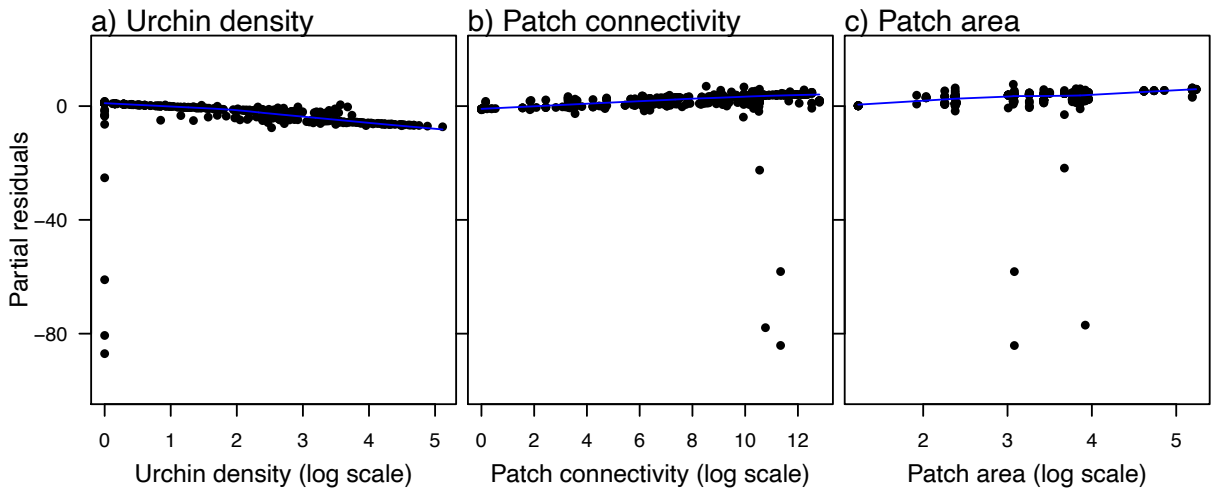

Figure S11: GLMM partial residuals (Zuur et al. 2009) plotted against each fixed effect. LOESS smoothers are shown in blue.

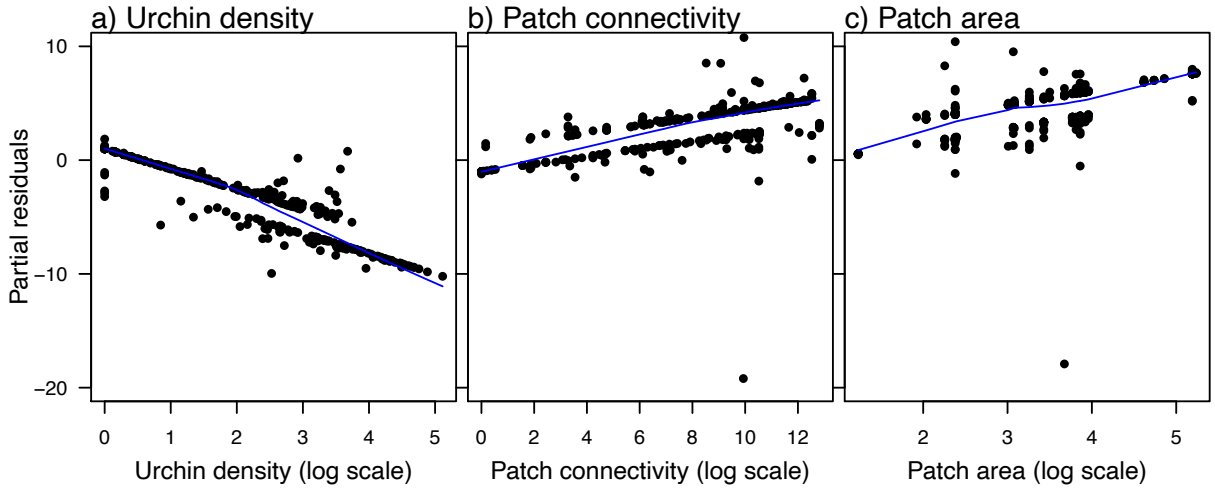

Figure S12: Partial residuals of the GLMM re-fitted without outliers plotted against each fixed effect. LOESS smoothers are shown in blue.

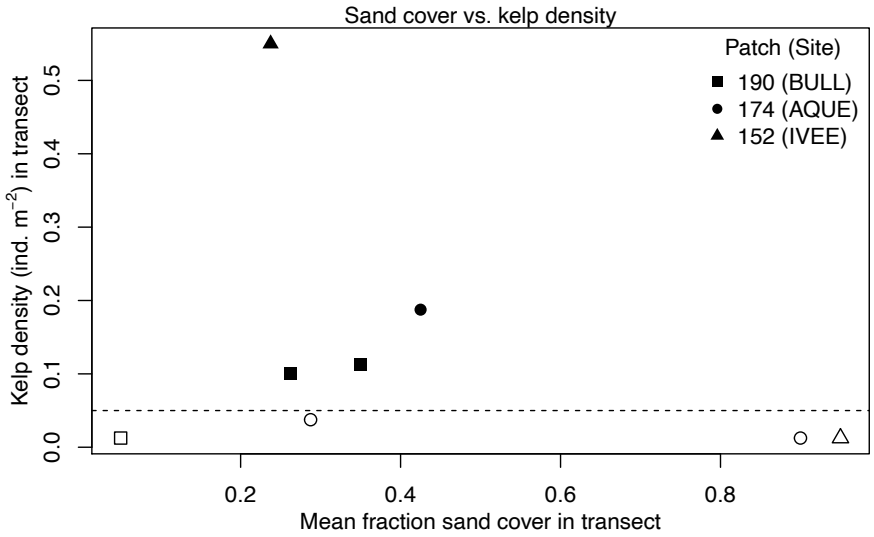

Figure S13: Sand cover plotted against observed kelp densities for the four outliers identified in the GLMM residuals (open symbols). Values for the other transects in the same patches and same years as these outlier transects are shown in black. The dashed horizontal line indicates the threshold for the high kelp state. The outlier transect in patch 152 (part of the LTER's IVEE site) and one of the outlier transects in patch 174 (part of the LTER's AQUE site) have higher sand cover than the other transect(s) in their respective patches, which accounts for why kelp was in the low state in these transects. (Daniel Reed, *pers comm*).

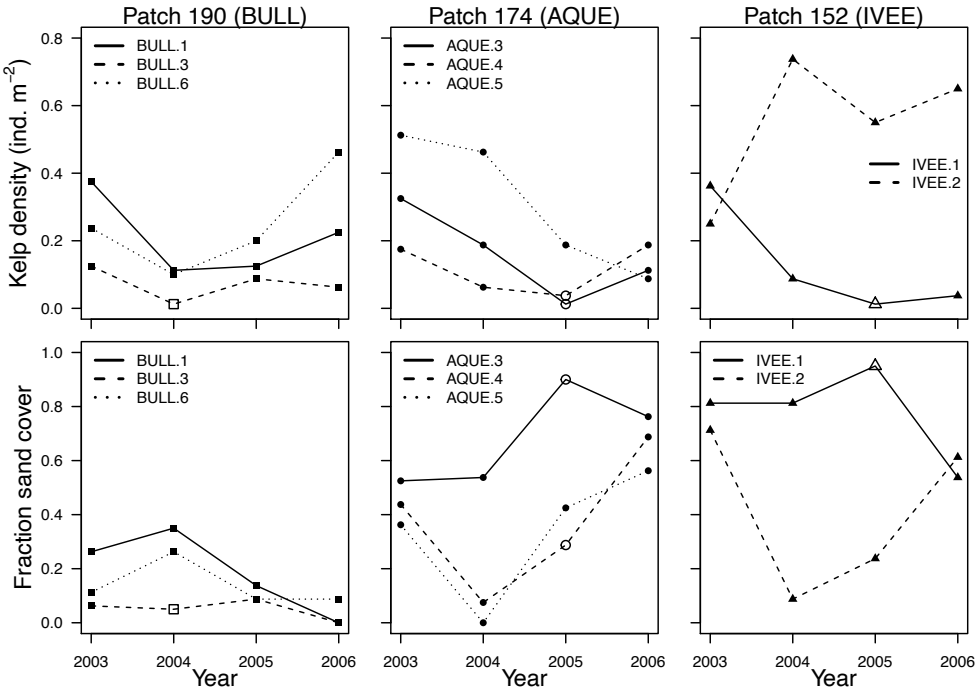

Figure S14: Kelp dynamics and sand cover in the outlier-containing patches around the time period in which the four residual outliers occurred. Each line represents a transect in the patch, with the kelp density and sand cover corresponding to the outliers marked with open symbols. As

suggested by Fig. S13, high sand cover appears to explain the outlier in patch 152. It may also explain the outliers in patch 174, as sand cover increased and kelp declined across all transects in this patch from 2004-2005. The transect AQUE.5 initially had higher kelp densities than the other two transects in patch 174, which could be why kelp in this transect remained above the threshold for the high state despite the increase in sand cover. However, sand does not appear to be responsible for the outlier in patch 190. Kelp densities declined slightly in all transects within this patch between 2003-2004, so the low kelp state observed in 2004 in transect BULL.3 could be a consequence of some larger-scale process affecting kelp throughout the patch.

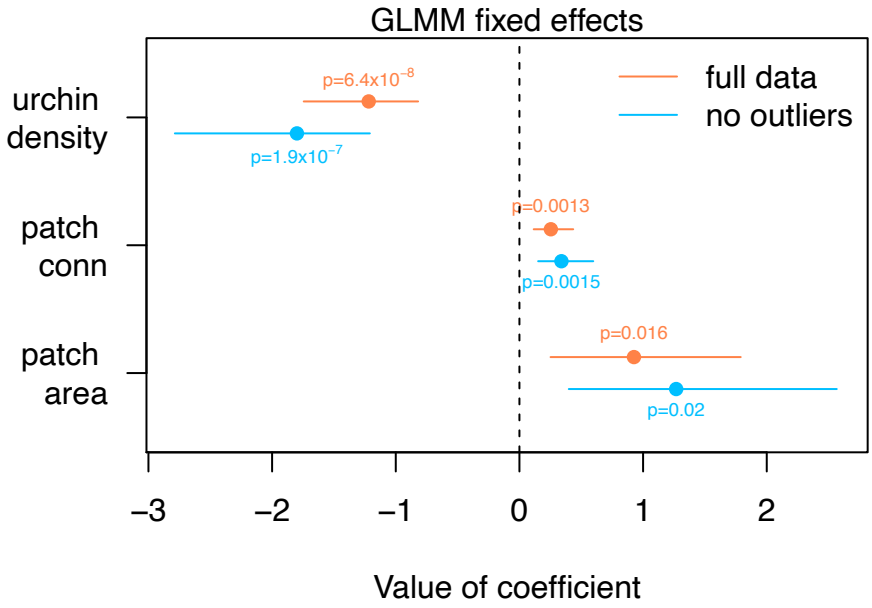

Figure S15: Estimated coefficients and bootstrapped 95% confidence intervals for the GLMM fit to the full data set (orange) and with outliers removed (blue). Note that fixed effects were not scaled prior to model fitting (to make comparison with the ODE model more intuitive); thus, the magnitudes of the coefficients within each model cannot be directly compared to one another.

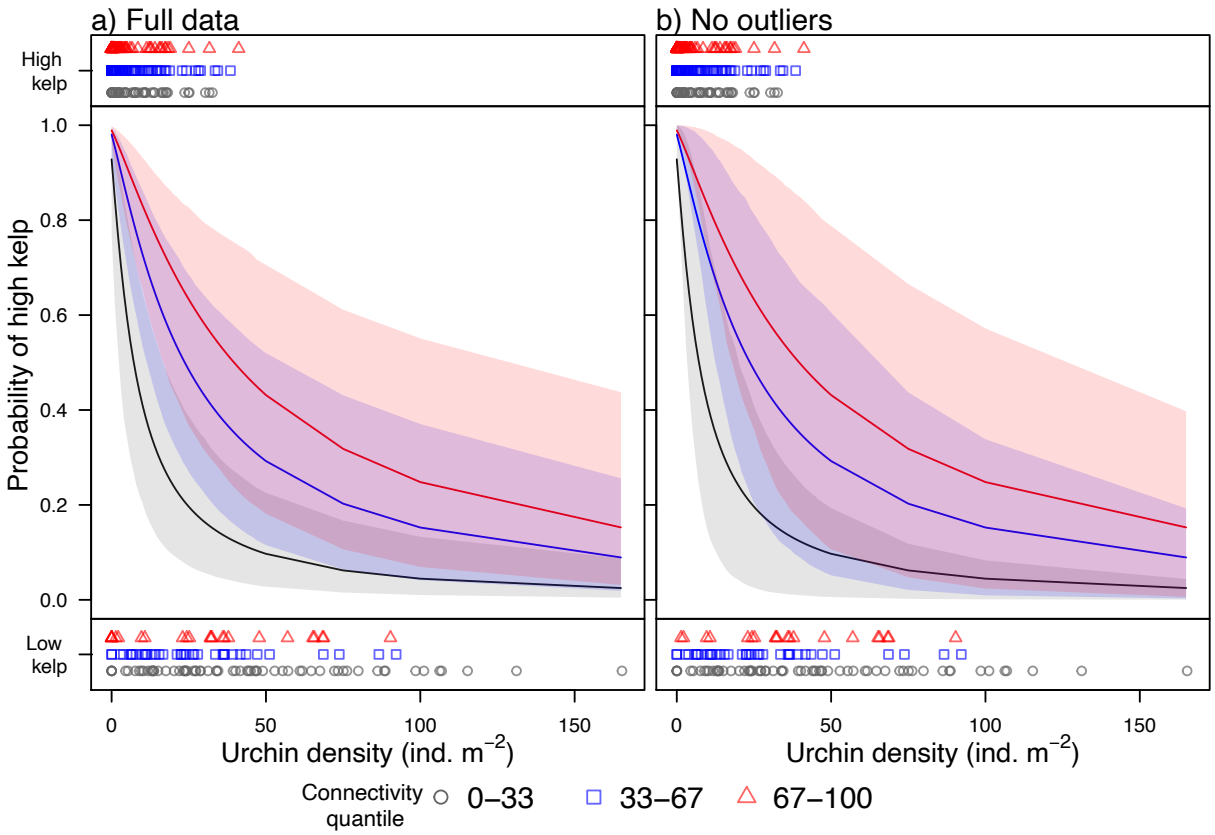

Figure S16: Predictions and bootstrapped 95% confidence intervals from the GLMM fit to a) the full data set and b) with outliers removed. Predictions are shown for the 15 (gray), 50 (blue), and 85% (red) quantiles of patch connectivity. The top and bottom panels show observations of kelp in the low and high state, respectively, broken up into the 0-33% quantile (gray circles), 33-67% quantile (blue squares), and 67-100% quantiles (red triangles) of patch connectivity. Based on Figure 4 of Castorani et al. (2015).

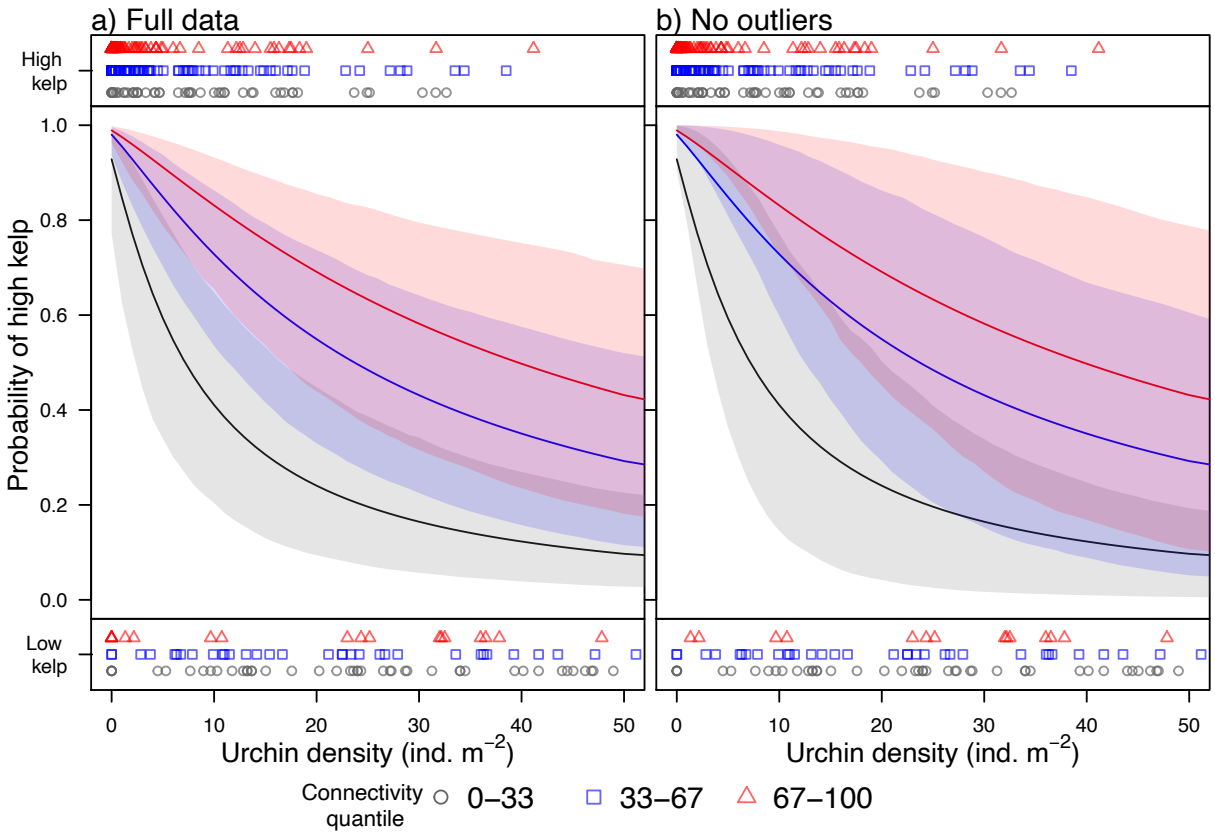

Figure S17: Same as Fig. S16 but only showing urchin densities from 0-50 individuals m^{-2} (the range used in the ODE validation simulations).

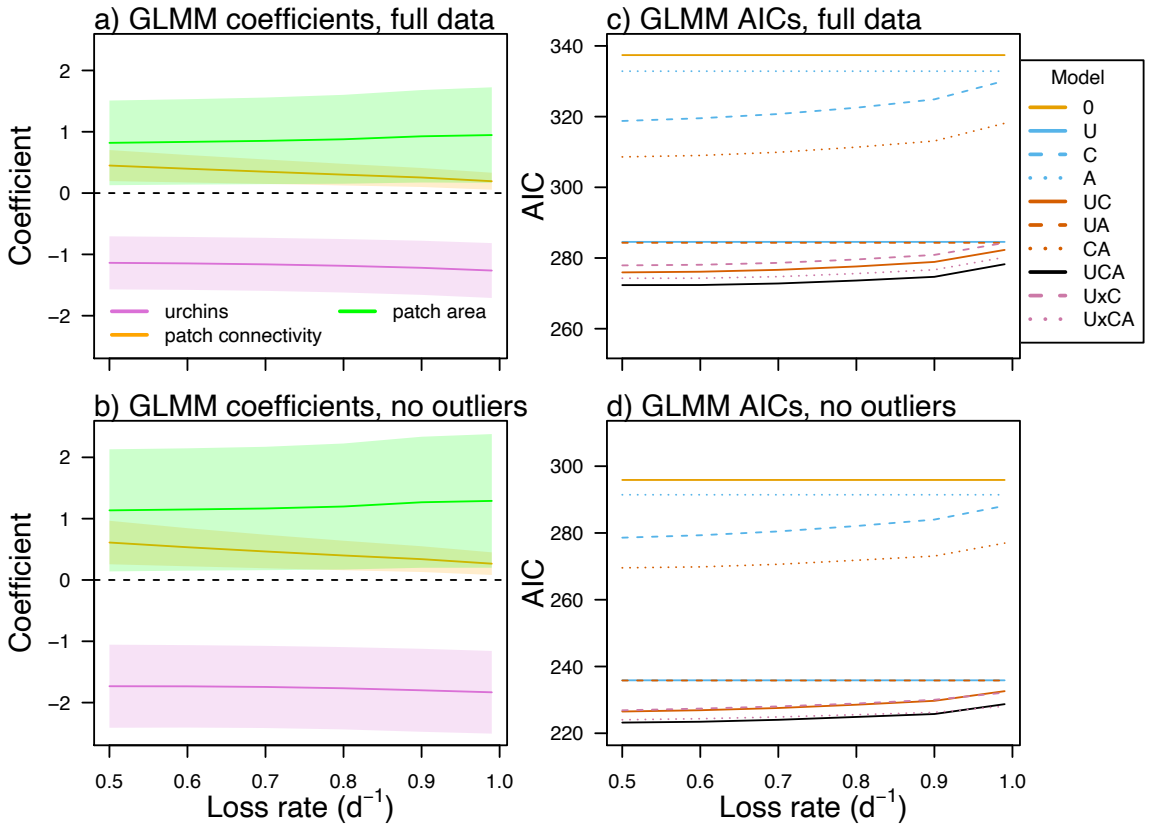

Figure S18: Sensitivity of GLMM estimates and model selection to the value of the loss rate λ used to calculate patch connectivity. In a-b), coefficient estimates and 95% confidence intervals are shown for the UCA model (independent fixed effects of urchin density, patch connectivity, and patch area). The top row shows results for GLMMs fit to the full dataset, while the bottom row shows results for GLMMs fit to the dataset with outliers removed.

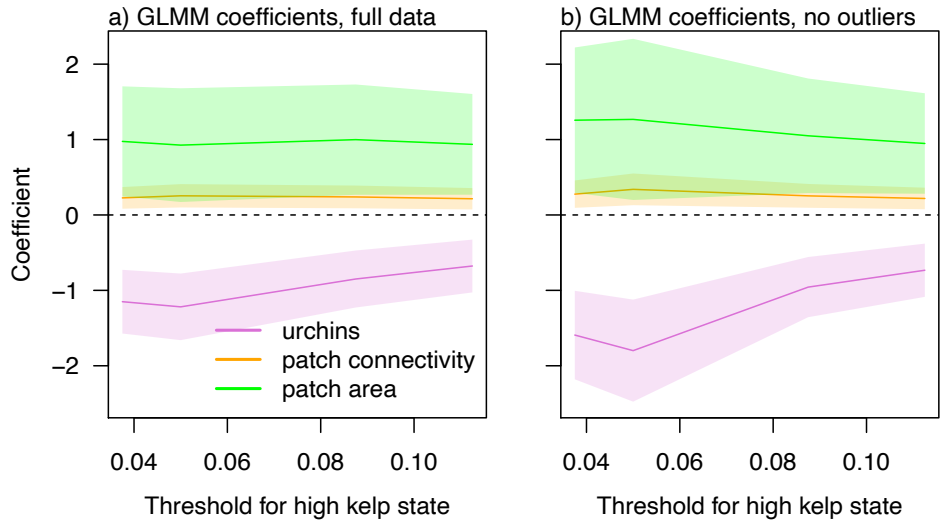

Figure S19: Effect of threshold for the high kelp state (kelp individuals m^{-2}) on estimates of GLMM fixed effect coefficients and 95% confidence intervals. Results are shown for the GLMM fit to a) the full dataset and b) the dataset with outliers removed. In both cases, the threshold did not affect the best-fitting GLMM, which included independent fixed effects of urchin density, patch connectivity, and patch area. There was a general reduction in urchin density's effect size with increasing threshold value, which is possibly because factors other than urchin grazing (e.g., sand inundation, poor recruitment) are more likely to cause kelp density to fall into the low state when the threshold is higher.

5. ODE-GLMM COMPARISON METHODS

5.1 Ensemble approach for connectivity parameters

To calculate rates of spores and drift input (the ODE parameters ε_s and ε_d, respectively) corresponding to observed values of patch connectivity, I used the following equations (also in Table 2):

$$\varepsilon_s = \sum_i \theta_i \omega_{si} \rho b_{Ci} (1-\lambda_{si})^{t_{sij}} / \exp(\text{area}_{lm}) \qquad \text{(S1)}$$

$$\varepsilon_d = \sum_i \theta_i \omega_{di} d b_{Ci} (1-\lambda_{di})^{t_{dij}} / \exp(\text{area}_{lm}) \qquad \text{(S2)}$$

Where b_{Ci} is the observed canopy biomass in source patch i, and $area_{lm}$ is the area of the destination patch on the log-scale. When generating predictions from the GLMM, I used observed values of patch connectivity but set patch area equal to its mean value on the log-scale (allowing me to isolate effects of connectivity). Therefore, in the above equations, I assumed all destination patches had an area of $area_{lm}$ = exp(mean(log(*patch area*))), where *patch area* are the observed patch areas in the empirical dataset.

The remaining elements in eqn.s S1-2, defined in Table S4, are themselves parameters that needed to be estimated. To propagate uncertainty in these estimates through to calculations of ε_s and ε_d, I used an ensemble approach in which I drew values of each parameter from a probability distribution that, when possible, incorporated available information on the parameter's potential values. Data on distributions of drift production rates (d) and the fraction of total kelp biomass in the canopy (θ^{-1}) were available from SBC LTER data (SBC LTER et al. 2023a). For spore connectivity, I followed existing studies and set the expected values of dispersal times equal to the observed ROMS times. I also chose an expected value of 0.9 d^{-1} for spore loss rate, as this produces spore dispersal distances consistent with empirical estimates (Castorani et al. 2015). The remaining parameters had greater uncertainty, so I chose broad distributions to capture a range of possible values. In the case of drift dispersal times, I still assumed an underlying linear relationship with the ROMS times (as these are indicative of oceanographic distances between patches; Mitarai et al. 2009), but allowed the slope of this relationship to vary uniformly from 0.5-1.5 (with slopes <1 indicating drift travels faster than the Lagrangian particles, e.g., due to wind along the surface, and slopes >1 indicating drift travels slower, e.g., due to drag).

For a given value of patch connectivity (e.g., the 10% quantile of observed values), I generated 40,000 values each of ε_s and ε_d using the following steps: 1) draw a single value each of ρ, d, v, and β , 2) draw values of θ^{-1} , ω_{si} , ω_{di} , λ_{si}, λ_{di}, t_{sij}, and t_{dij} for each source patch i, 3) calculate potential connectivity and export rates of spores and drift using the results of steps 1-2, 4) repeat 200 times, 5) multiply the resulting set of 200 potential connectivities and 200 export rates together and for each combination sum across all source patches to produce a value of ε_s and ε_d. I then used various quantiles from the resulting sets of ε_s and ε_d parameter values in my ODE simulations (Fig. 6, Fig. S23).

Table S4: Distributions of the intermediate parameters used to calculate values of spore and drift connectivity. t_{ROMSij} indicates the ROMS-derived dispersal time from patch i to j. When necessary, values were truncated to remain within possible ranges for each parameter (i.e., all positive, between 0 and 1 for parameters representing fractions).

Parameter	Description	Units	Distribution
θ_i^{-1}	Fraction of kelp biomass in patch i located in the canopy	–	Normal(0.3, 0.15)
ω_{si}	Fraction of locally produced spores exported from patch i	–	Normal(0.25, 0.1)
ω_{di}	Fraction of locally produced drift exported from patch i	–	Normal(0.25, 0.1)
ρ	Spore production rate	spores kg^{-1} d^{-1}	Uniform(1, 100)
d	Drift production rate	kg drift kg^{-1} d^{-1}	LogNormal(-3.7, 0.5)
λ_{si}	Spore proportional loss rate	d^{-1}	Normal(0.9, 0.01)
λ_{di}	Drift proportional loss rate	d^{-1}	Normal(v, 0.025); v ~ Normal(0.75, 0.2)

t_{sij}	Spore dispersal time from patch i to j	d	Normal(t_{ROMSij}, 0.01)
t_{dij}	Drift dispersal time from patch i to j	d	Normal($\beta * t_{ROMSij}$, 0.1); $\beta \sim$ Uniform(0.5, 1.5)

5.2 Random effect parameters

To estimate distributions of the random effect parameters (Table 2, Table S5), I used SBC LTER and CINP KFMP data on kelp plant size and densities of juvenile kelp from the transects and years in the GLMM dataset, as well as regional data on swell heights during this same time period (SBC LTER et al. 2022a, SBC LTER et al. 2022c, Kushner et al. 2013, Bell 2023). Plant size is recorded as the number of fronds per plant, which I converted to biomass using published relationships between frond density and plant biomass (Rassweiller et al. 2018, SBC LTER et al. 2023a). I chose values of *b* (biomass per plant) equal to the means of the quintiles of observed plant masses (Table S5). As these represent quintiles, I assumed each value occurred in 20% of observations. I used the data on juvenile kelp densities to approximate recruitment conditions, which are captured in my ODE model by initial conditions, mortality rates, and maturation rates of gametophytes and juvenile sporophytes. I assumed observations of zero juveniles m^{-2} indicate poor recruitment (with mortality rates = 2x times default values and maturation rates = 0.2 x times default values), observations greater than 0 but less than the 80% quantile of non-zero values indicate intermediate recruitment, and observations above this quantile indicate favorable recruitment (Table S5). Based on these classifications, poor, intermediate, and favorable recruitment conditions occurred in 40, 48, and 12% of observations, respectively. Finally, I used the swell height data to infer disturbance regimes at each transect during the study period. These data are derived from a spectral refraction wave hindcast model (outputs provided by the Coastal Data Information Program; http://cdip.ucsd.edu/MOP_v1.1/) and have been formatted to give maximum quarterly swell heights in 30 x 30m Landsat pixels across southern California (Bell 2023). I selected pixels that contained the focal transects and determined the number of severe storms that occurred in each of these pixels during the study period. Severe storms were defined as maximum swell heights of ≥2.5m (the threshold at which negative relationships with canopy biomass have been observed; Bell et al. 2015). These storms were represented in my ODE simulations by an indicator parameter I_{storm}, where $I_{storm} = 1$ meant that the system experienced a severe winter disturbance that removed 90% of existing giant kelp and $I_{storm} = 0$ meant there was no severe disturbance. I found that across all focal transects, severe storms occurred approximately once every 4 years on average, and therefore assumed $I_{storm} = 1$ and $I_{storm} = 0$ occurred at frequencies of 0.25 and 0.75, respectively.

Table S5. Random effect parameters used in the ODE simulations. Default values of maturation and mortality parameters are given in Table 1 in the main text.

Parameter(s)	Description	Values	Frequencies
b	Biomass per kelp plant (proxy for productivity)	{1.8, 4.2, 7.4, 12.8, 34.4}	{0.2, 0.2, 0.2, 0.2, 0.2}
G_0, J_0, r_G, r_J, μ_G, μ_J	Initial conditions, maturation rates, and mortality rates of early life stages (proxy for recruitment conditions)	{poor, intermediate, favorable}: G_0 = {0, 2.6, 16.6}, J_0 = {0, 1.3, 8.3}, r_G & r_J = {0.2, 1, 1.2}x defaults, μ_G & μ_J = {2, 1, 0.5}x defaults	{0.4, 0.48, 0.12}
I_{storm}	Indicator of whether a severe storm occurred (proxy for disturbance regime)	{no storm, storm}: I_{storm} = {0,1}	{0.75, 0.25}

The resulting sets of random effect parameters and their corresponding frequencies are summarized in Table S5. These produced a total of 30 random effect parameter combinations, each representing possible environmental conditions in a given transect and year. I used these random effect parameters to generate predictions from my ODE model that approximate the effects of urchins and connectivity on giant kelp in an otherwise average transect and year (see Fig. S20). My first step was to select values of the fixed effect parameters u, ε_s and ε_d. As an example, for Fig. S20 I chose a set of 20 urchin densities between 0-50 urchins m^{-2} and no connectivity ($\varepsilon_s = \varepsilon_d = 0$). For each combination of these fixed effect parameters (eg., u =10, $\varepsilon_s = \varepsilon_d = 0$), I ran the ODE model with all possible combinations of random effect parameters in Table S5. Each of these simulations produced a value of A_{0min}, the minimum initial kelp density above which kelp would be in the high state (>0.05 individuals m^{-2}) at the end of one year (Fig. S20a-c, see main text for more details). I used the distribution of observed kelp densities during the study period (Fig. S21) to convert these A_{0min} values into probabilities that kelp would be in the high state at the end of the simulated year (Fig. S20 d-f). Finally, I weighted the results for each random effect combination i by the joint probability of that combination occurring (i.e., the product of the probabilities of each value in that combination occurring) and summed across all possible random effect combinations. This resulted in a single weighted average of the probability that kelp would be in the high state for a given set of u, ε_s and ε_d values (Fig. S20g).

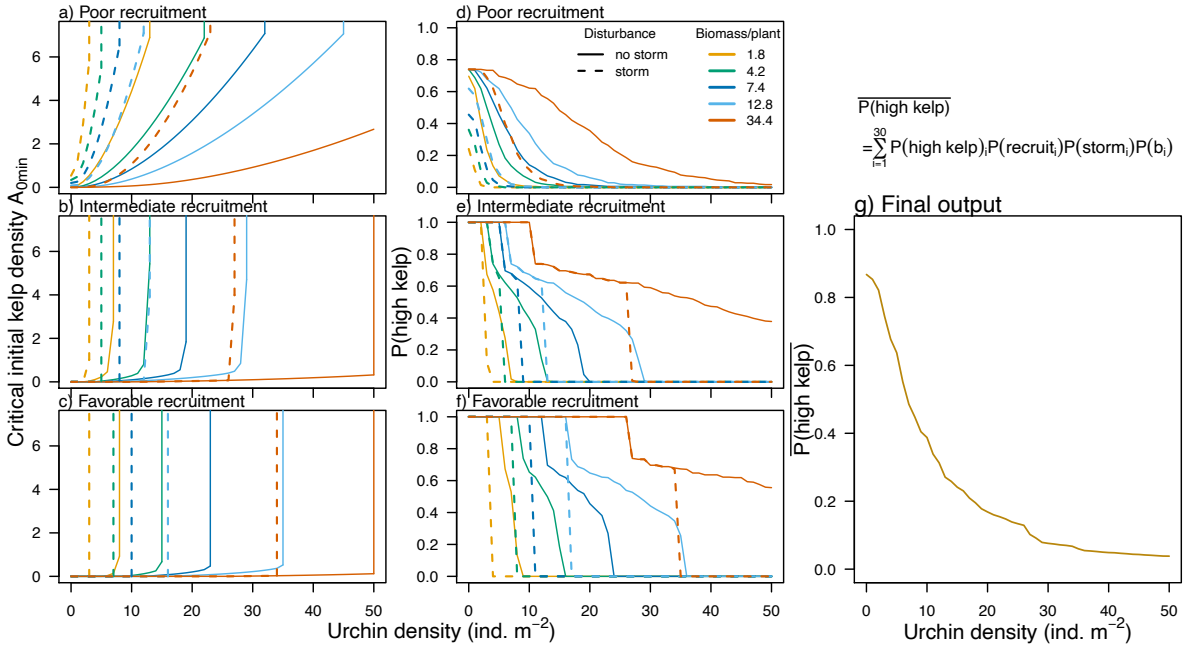

Figure S20: Example of how random effect parameters were averaged to produce a single prediction from the ODE model. Here, connectivity parameters ε_s and ε_d were both zero in all simulations. The ODE model was simulated for all possible combinations of recruitment conditions (rows 1-3), storm disturbance (line type) and biomass per plant b (line color). For each combination, A_{0min} was computed (a-c) and converted to the probability of kelp being in the high state (d-f). The outputs for each parameter combination were then weighted by the joint probability of that combination occurring (see Table S5) and summed to produce and average probability of kelp being in the high state (g).

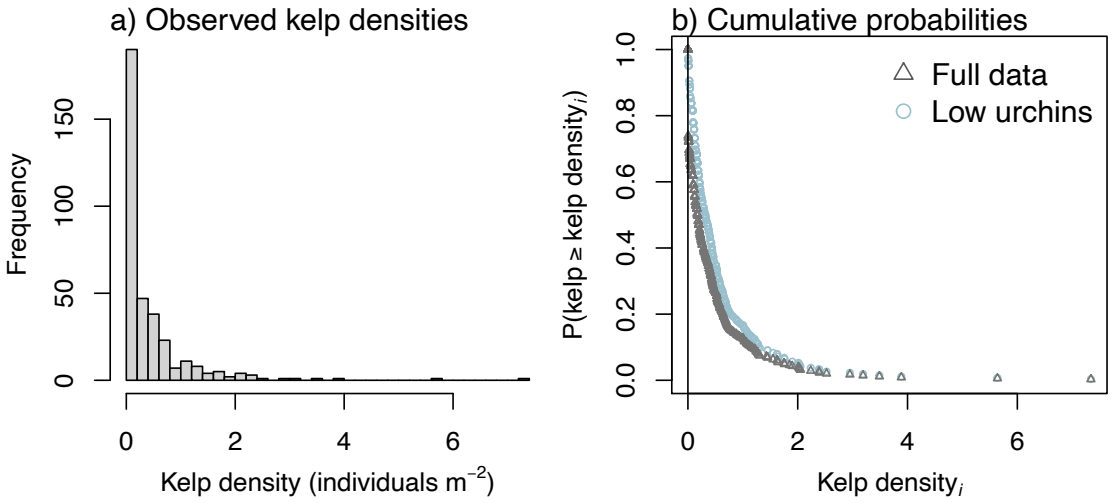

Figure S21: a) Distribution of kelp densities in the data set used to fit the GLMM. b) Probabilities of kelp density being greater than or equal to a given density i, calculated as the

fraction of observed densities greater than or equal to the ith density. Probabilities were calculated using the full dataset (gray triangles) and again using the subset of the data with urchin densities less than 25 individuals m^{-2} (the 75th quantile of observed urchin densities in the data; blue circles). The probabilities calculated using the full data set were used to convert initial kelp densities predicted by my ODE model into probabilities of kelp being in the high state (Fig. S20).

Assumptions

A key assumption of the methods described above is that the probability of a given value of a random effect parameter occurring is independent of the other random and fixed effect parameter values. Furthermore, my conversion from A_{0min} to Pr(high kelp) assumes the distribution of possible initial kelp densities is not strongly affected by values of the fixed and random effect parameters in the subsequent year. In reality, many of the processes represented by these parameters could interact with each other as well as influence initial kelp abundance (e.g., high urchin densities in the simulation year might indicate urchin densities were also high the previous year, making high initial kelp densities less likely). However, I found there were generally no strong relationships between any of my parameter values (Fig. S22). Furthermore, restricting my data set to observations with relatively low urchin densities had only minor effects on the distribution of initial kelp densities (Fig. S21b), suggesting my estimates of Pr(high kelp) are fairly robust. Thus, I concluded my simplified approach produced a reasonable approximation of the study region and time period used in this study.

I also made several assumptions regarding local dynamics in each ODE simulation. In particular, I ignored potential intra-annual fluctuations in my fixed and random effect parameters. This was because, for most of these parameters, data was only available at a single time point each year and I therefore could not estimate changes in their values over shorter timescales. However, I did incorporate some seasonal dynamics in my simulations by increasing the background mortality rate of adult giant kelp, μ_A, from 0.001 to 0.007 during winter months (representing mild to intermediate intensity winter storms). Data to inform these dynamics were available from the SBC LTER, which has estimated monthly kelp plant loss rates at three sites along the Santa Barbara coast since 2002 (SBC LTER et al. 2023a).

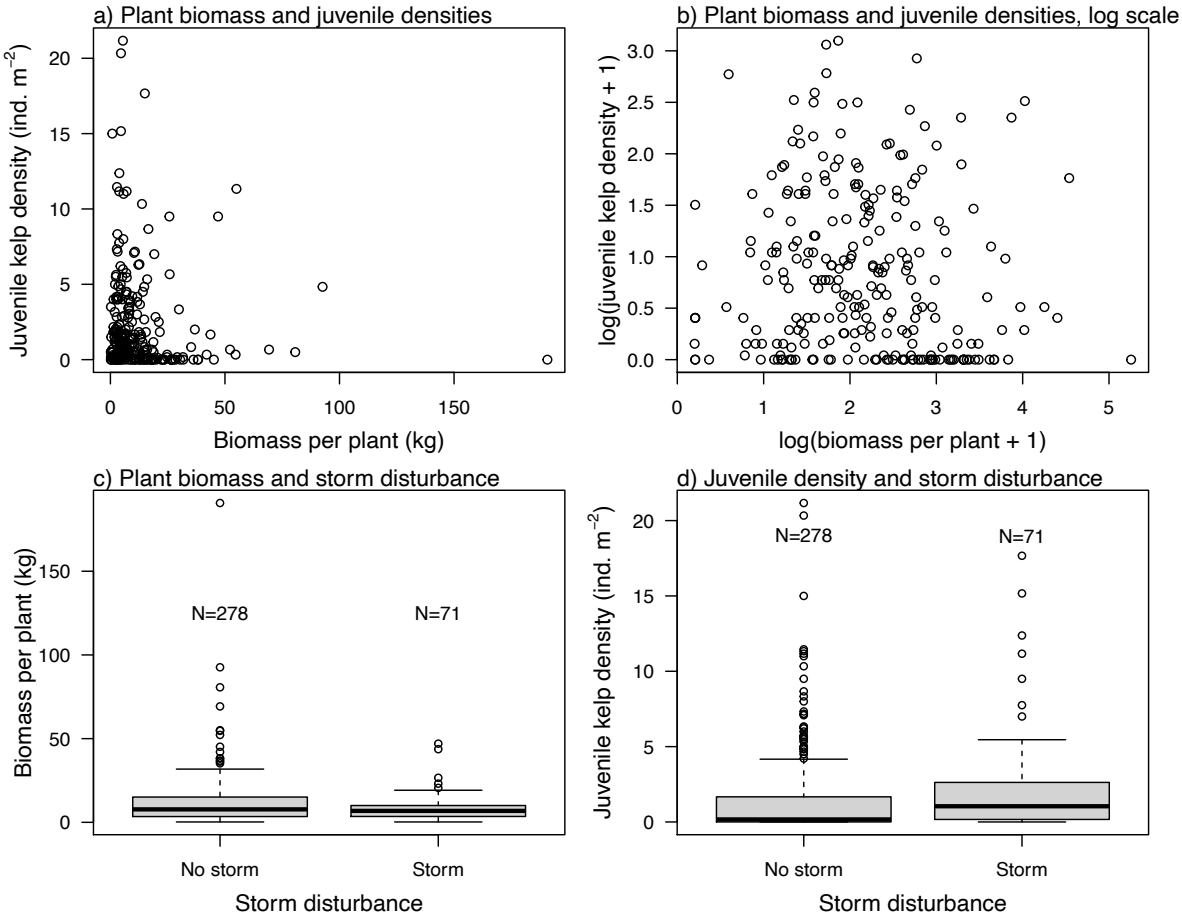

Figure S22: Relationships between values of random effect parameters (with juvenile densities serving as a proxy for recruitment conditions). a) and b) show the relationship between mean biomass per adult kelp plant and density of juvenile kelp on the raw scale (a) and log scale (b). The raw data suggest a potential negative relationship between adult biomass and juvenile densities (possibly because larger plants shade the bottom and cause early life stages to be light-limited; Graham et al. 1997); however, this pattern appears to be largely driven by a few extreme observations and is not apparent in the log transformed data. c) and d) show the distribution of mean biomass per plant values and juvenile kelp densities, respectively, in transects and years that did or did not experience a severe storm event (i.e., maximum swell height of at least 2.5m). I note that effects of storm disturbance could be stronger than suggested here, as it is possible the system had recovered by the time the transects were surveyed in late summer. However, in my ODE model, disturbance occurred several months after the start of each simulation, and therefore shouldn't affect initial juvenile densities or biomass per plant.

5.3 Supplemental results

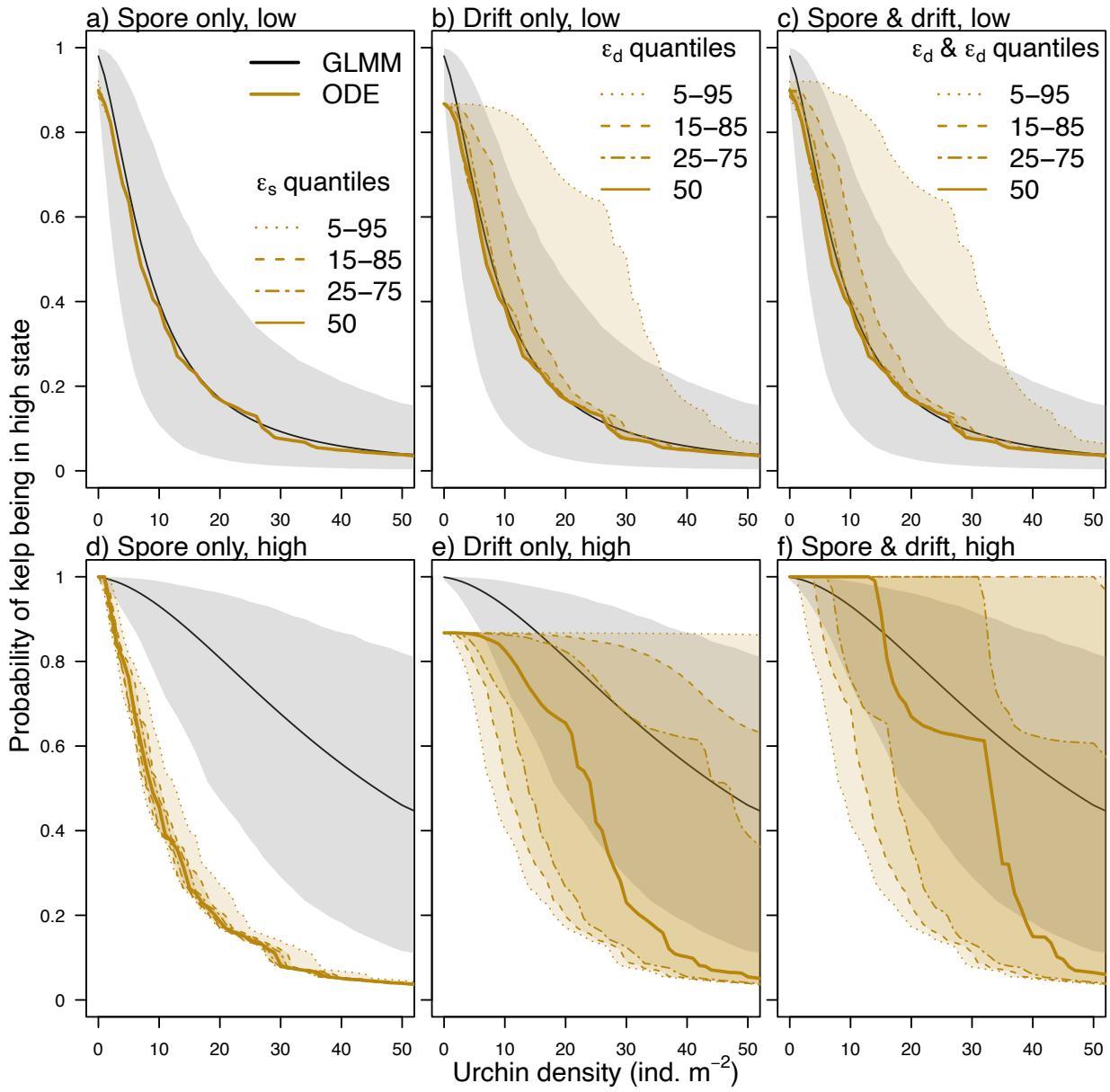

Figure S23: Same as Figure 6 in the main text, but with results shown for additional quantiles of simulated ε_s and ε_d values.

6. DRIFTER ANALYSES

Ohlmann 2019 used GPS drifters to record the paths of approximately 200 detached kelp plants along the Santa Barbara coastline. Plants were tagged monthly between November 2015 and December 2017 and tracked from their starting locations (one of three kelp forests off the coast of Santa Barbara) until they either washed ashore or began to leave the Santa Barbara Channel. The GPS instruments transmitted their positions every 10 minutes, providing detailed tracks of each drifting plant's path (Fig. S24). See Ohlmann 2019 for more details on the methods.

I overlaid the tracks of each tagged plant with the locations of the kelp metapopulation patches identified by Cavanaugh et al. (2014) and calculated the number of patches each individual plant's path intersected. I found that 56% of plants moved through at least two patches, with one plant moving through a total of 6 patches (Fig. S25). The average distance between the first and last patch encountered by a kelp plant was 3.5 km. Thus, these data indicate exported drift kelp is not always immediately transported offshore or deposited on beaches, and may instead travel to neighboring kelp forests (although whether buoyant drift like the plants tracked here can become available to benthic urchins in recipient patches will require more studies).

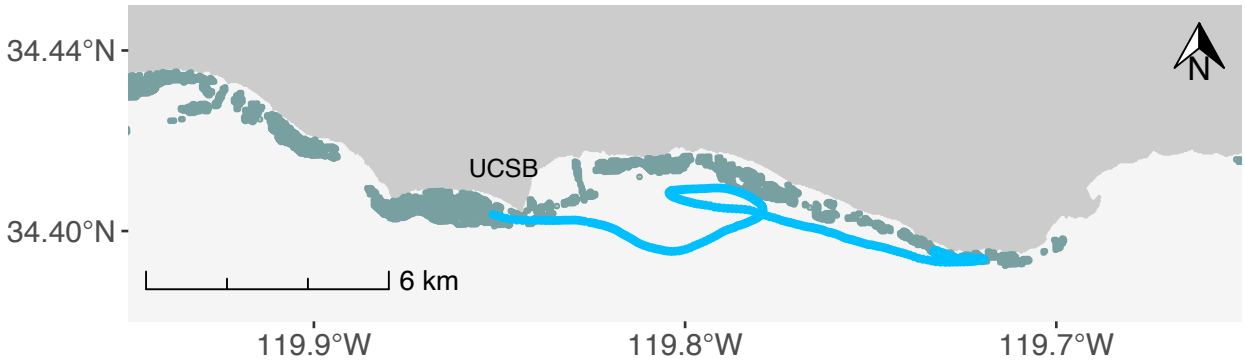

Figure S24: Example of a drifter track (blue) recorded by Ohlmann (2019) along the coast near the University of California, Santa Barbara. Kelp metapopulation patches are shown in dark teal.

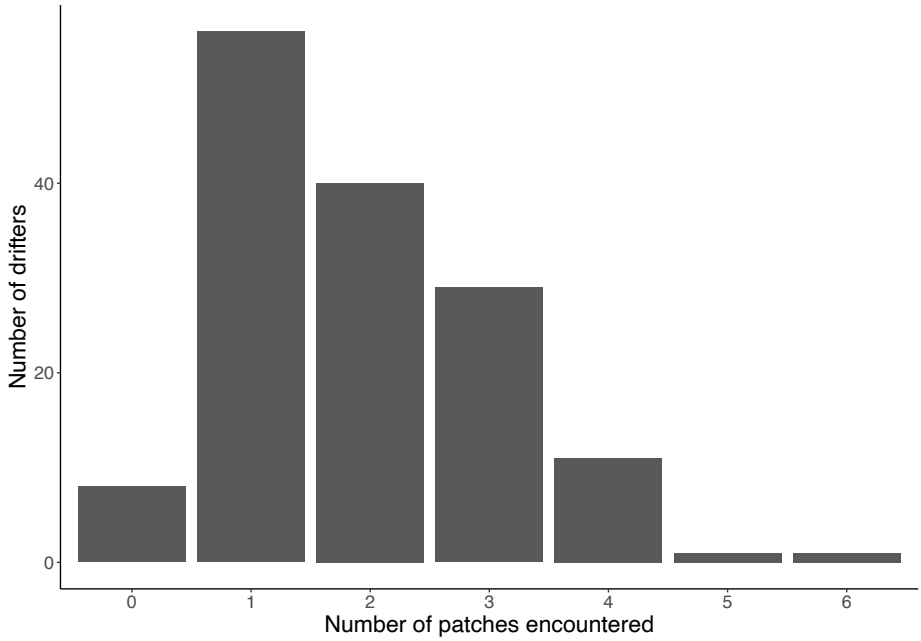

Figure S25: Histogram of the number of metapopulation patches encountered by individual tagged drifting kelp plants (including patches of origin, for plants that were tagged within patches).

LITURATURE CITED

Bell, TW (2023) SBC LTER: Reef: California kelp canopy and environmental variable dynamics ver 1. Environmental Data Initiative. https://doi.org/10.6073/pasta/c40db2c8629cfa3fbe80fdc9e086a9aa

Bell TW, Cavanaugh KC, Reed DC, Siegel DA (2015) Geographical variability in the controls of giant kelp biomass dynamics. J Biogeogr 42:2010–2021.

Castorani MCN, Bell TW, Walter JA, Reuman DC, Cavanaugh KC, Sheppard LW (2022a) Disturbance and nutrients synchronise kelp forests across scales through interacting Moran effects. Ecol Lett: ele.14066.

Castorani MCN, Reed DC, Alberto F, Bell TW, Simons RD, Cavanaugh KC, Siegel DA, Raimondi PT (2015) Connectivity structures local population dynamics: a long-term empirical test in a large metapopulation system. Ecology 96:3141–3152.

Castorani MCN, Reed DC, Raimondi PT, Alberto F, Bell TW, Cavanaugh KC, Siegel DA (2022b) Kelp metapopulations: Semi-annual time series of giant kelp patch area, biomass and fecundity in southern California, 1996 – 2006 ver 2. Environmental Data Initiative. https://doi.org/10.6073/pasta/4c5a27154458ece5585384339eb0c2ee (accessed 15 April 2023)

Castorani MCN, Reed DC, Raimondi PT, Alberto F, Bell TW, Cavanaugh KC, Siegel DA, Simons RD (2017) Fluctuations in population fecundity drive variation in demographic

connectivity and metapopulation dynamics. Proc R Soc B 284:20162086.

Castorani MCN, Siegel DA, Simons RD, Reed DC, Raimondi PT, Alberto F (2022c) Kelp metapopulations: Semi-annual time series of spore dispersal times among giant kelp patches in southern California, 1996 – 2006 ver 4. Environmental Data Initiative. https://doi.org/10.6073/pasta/d1107107e7c9ebc6476dfbe9e64eb6cb (accessed 15 April 2023)

Cavanaugh K, Siegel D, Reed D, Dennison P (2011) Environmental controls of giant-kelp biomass in the Santa Barbara Channel, California. Mar Ecol Prog Ser 429:1–17.

Cavanaugh KC, Siegel DA, Raimondi PT, Alberto F (2014) Patch definition in metapopulation analysis: a graph theory approach to solve the mega-patch problem. Ecology 95:316–328.

Cavanaugh KC, Siegel DA, Raimondi PT, Alberto F (2019) SBC LTER: Spatial definitions of giant kelp (Macrocystis pyrifera) patches in southern and central California ver 2. Environmental Data Initiative. https://doi.org/10.6073/pasta/97ef540ba3fc62dff50779533bb39466 (accessed 15 April 2023)

Dayton PK, Currie V, Gerrodette T, Keller BD, Rosenthal R, Tresca DV (1984) Patch dynamics and stability of some California kelp communities. Ecol Monogr 54:253–289.

Deysher LE, Dean TA (1984) Critical irradiance levels and the interactive effects of quantum irradiance and dose on gametogenesis in the giant kelp, Macrocystis pyrifera1. J Phycol 20:520–524.

DiFiore B, Rennick M, Curtis J, Reed DC, Stier A (2021) SBC LTER: Sea urchin foraging rates on giant kelp ver 1. Environmental Data Initiative. https://doi.org/10.6073/pasta/6af4cc3b0e63b887baf1ae9201e1cd1d (accessed 15 April 2023)

Dong C, Idica EY, McWilliams JC (2009) Circulation and multiple-scale variability in the Southern California Bight. Prog Oceanogr 82:168–190.

Graham M, Harrold C, Lisin S, Light K, Watanabe J, Foster M (1997) Population dynamics of giant kelp Macrocystis pyrifera along a wave exposure gradient. Mar Ecol Prog Ser 148:269–279.

Harrold C, Pearse JS (1987) The ecological role of echinoderms in kelp forests. Echinoderm Studies 2:137–233.

Karatayev VA, Baskett ML, Kushner DJ, Shears NT, Caselle JE, Boettiger C (2021) Grazer behaviour can regulate large-scale patterning of community states. Ecol Lett 24:1917–1929.

Kushner D, Rassweiler A, McLaughlin JP, Lafferty KD (2013) A multi-decade time series of kelp forest community structure at the California Channel Islands. Ecology 94:2655.

Mitarai S, Siegel DA, Watson JR, Dong C, McWilliams JC (2009) Quantifying connectivity in the coastal ocean with application to the Southern California Bight. J Geophys Res 114:C10026.

Nisbet RM, Bence JR (1989) Alternative dynamic regimes for canopy-forming kelp: a variant on

density-vague population regulation. Am Nat 134:377–408.

Ohlmann C (2019) Data from freely drifting kelp plants tagged with drifters in the Santa Barbara Channel between November of 2015 and December of 2017. Biological and Chemical Oceanography Data Management Office. https://doi.org/10.1575/1912/bco-dmo.739111.1 (accessed 15 April 2023)

Rassweiler A, Reed DC, Harrer SL, Nelson JC (2018) Improved estimates of net primary production, growth, and standing crop of *Macrocystis pyrifera* in Southern California. Ecology 99:2132–2132.

Reed DC (1990) The effects of variable settlement and early competition on patterns of kelp recruitment. Ecology 71:776–787.

Reed DC, Laur DR, Ebeling AW (1988) Variation in algal dispersal and recruitment: the importance of episodic events. Ecol Monogr 58:321–335.

Reed DC, Lewis RJ, Anghera M (1994) Effects of an open-coast oil-production outfall on patterns of giant kelp (Macrocystis pyrifera) recruitment. Mar Biol 120:25–31.

Reed DC, Rassweiler A, Carr MH, Cavanaugh KC, Malone DP, Siegel DA (2011) Wave disturbance overwhelms top-down and bottom-up control of primary production in California kelp forests. Ecology 92:2108–2116.

SBC LTER, Rassweiler AA, Harrer S, Reed DC, Nelson CJ, Miller RJ (2023a) SBC LTER: REEF: Net primary production, growth and standing crop of Macrocystis pyrifera in Southern California ver 7. Environmental Data Initiative. https://doi.org/10.6073/pasta/1dcf59ef5a7ec3fd7c90203e3a2c171a (accessed 15 April 2023)

SBC LTER, Reed DC, Miller RJ (2022a) SBC LTER: Reef: Kelp Forest Community Dynamics: Abundance and size of Giant Kelp (Macrocystis Pyrifera), ongoing since 2000 ver 26. Environmental Data Initiative. https://doi.org/10.6073/pasta/7d7b640d5cafd29c00a647f6016e165d (accessed 15 April 2023)

SBC LTER, Reed DC, Miller RJ (2022b) SBC LTER: Reef: Kelp Forest Community Dynamics: Cover of sessile organisms, Uniform Point Contact ver 31. Environmental Data Initiative. https://doi.org/10.6073/pasta/7b9f59d4875c4e235448dd42ff7044ad (accessed 15 April 2023)

SBC LTER, Reed DC, Miller RJ (2022c) SBC LTER: Reef: Kelp Forest Community Dynamics: Invertebrate and algal density ver 29. Environmental Data Initiative. https://doi.org/10.6073/pasta/da35d83d200341c27ce50348e1835971 (accessed 15 April 2023)

SBC LTER, Reed DC, Miller RJ (2023b) SBC LTER: Reef: Kelp Forest Community Dynamics: Transect depth data ver 10. Environmental Data Initiative. https://doi.org/10.6073/pasta/1aed976cbe5c1fef745fc50e3d217747 (accessed 20 May 2023)

SCB MBON, Miller RJ, Rassweiler AR, Caselle J, Kushner D, Reed DC, Lafferty KD, Kui L,

O'Brien M (2021) Santa Barbara Channel Marine BON: Nearshore kelp forest integrated fish, 1981-ongoing ver 4. Environmental Data Initiative. https://doi.org/10.6073/pasta/dbf98d8ddc5f48c4bc074ae4293d8d7c (accessed 15 April 2023)

Zuur AF, Ieno EN, Walker N, Saveliev AA, Smith GM (2009) Mixed effects models and extensions in ecology with R. Springer New York, New York, NY.